Two-Dimensional MEMS Stage Integrated With Microlens Arrays for Laser Beam Steering

Sertan Kutal Gokce, Sven Holmstrom, Cyrille Hibert, Selim Olcer, David Bowman, and Hakan Urey

***Abstract*—A novel microelectromechanical stage with one uniaxial set of combs capable of 2-D actuation is presented. A polymer microlens array (MLA) is mounted vertically onto the stage. Driven at resonance, the stage deflects 124 μm out of plane and 34 μm in plane. Finally, laser beam steering is demonstrated using two cascaded MLAs. [2010-0201]**

***Index Terms*—Beam steering, comb drive, endoscopic imaging, microelectromechanical systems (MEMS) stage, microlens array (MLA).**

I. Introduction

Laser scanning with microelectromechanical system (MEMS) mirrors is used in many display and imaging applications [1]–[6]. These systems typically utilize mirrors to steer the beam and thus require beam folding. There are applications, such as the forward-looking endoscopic imaging probe, where the system needs to fit in a tiny tube. Achieving a large clear optical aperture is a challenge for mirror-based systems. High-resolution laser beam steering using one moving microlens array (MLA) and two stationary MLAs, where each is separated by one focal length, has been demonstrated by our group as well as other researchers [7]–[9]. Beam steering with single microlenses integrated into a microoptoelectromechanical system (MOEMS) has also been demonstrated [10]–[13]. With MLAs, large-angle beam steering can be achieved using in-line optics and only small lateral displacements. One major limitation is the discrete addressing problem, which can be solved by adding a millimeter-sized movable prescan lens (PSL) in the light train to continuously address any point along the scanline [7]. MLA scanning can achieve 1880 $\times$ 1880 resolvable spots with about $\pm$50-μm mechanical deflections in each axis using 20 $\times$ 20 arrays of microlenses across a 2 mm $\times$ 2 mm clear aperture [14]. The main drawbacks are the increased complexity of the system due to the need for an additional moving PSL and the limitations due to the diffraction-based operation principle. Fig. 1 shows the proposed compact MOEMS design for high-resolution beam steering.

The electrostatic comb-actuation principle is well known, and both in-plane [15] and out-of-plane [16] moving comb-drive actuators have been implemented. We developed a comb actuator that is capable of actuating in two axes simultaneously with only one set of combs. The new actuation principle, fabrication details, characterization, and the first laser beam steering demonstration results are reported.

Manuscript received July 1, 2010; revised September 28, 2010; accepted October 16, 2010. Date of publication November 29, 2011; date of current version February 2, 2011. This work was supported by The Scientific and Technological Research Council of Turkey (TÜBITAK) under Grant 106E068. Subject Editor O. Solgaard.

S. K. Gokce, S. Holmstrom, S. Olcer, and H. Urey are with Optical Microsystems Laboratory, Department of Electrical Engineering, Koç University, 34450 Istanbul, Turkey (e-mail: sergokce@ku.edu.tr; sholmstrom@ku.edu.tr; solcer@ku.edu.tr; hurey@ku.edu.tr).

C. Hibert is with Center of Micronanotechnology, Ecole Polytechnique Federale de Lausanne, 1015 Lausanne, Switzerland (e-mail: cyrille.hibert@epfl.ch).

D. Bowman is with Microvision, Inc., Redmond, WA 98052 USA (e-mail: david_bowman@microvision.com).

Color versions of one or more of the figures in this paper are available online at http://ieeexplore.ieee.org.

Digital Object Identifier 10.1109/JMEMS.2010.2090507

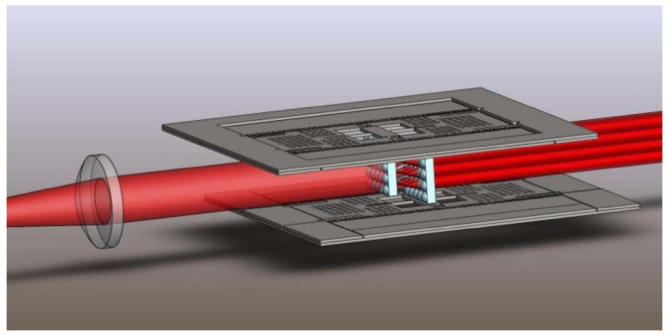

Fig. 1. Sketch of the proposed optical system. The laser is first collimated by a PSL. This collimated beam then passes through and is deflected by two MEMS stages, each carrying a perpendicularly mounted MLA.

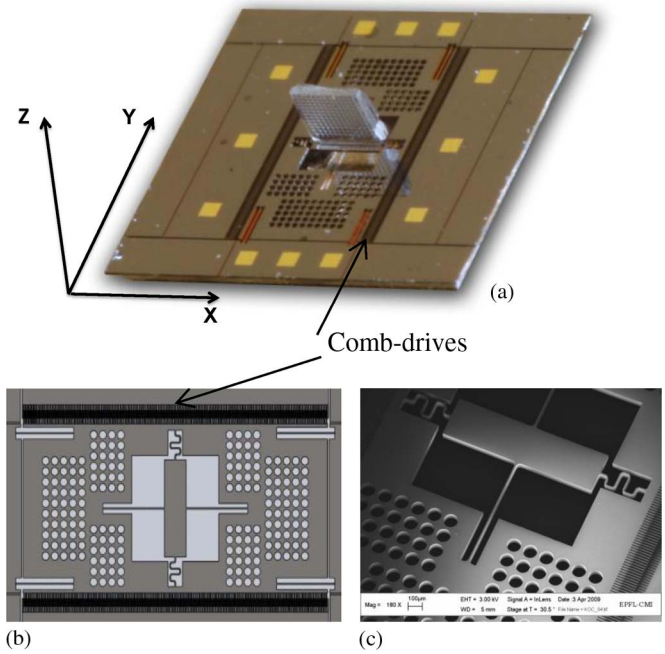

Fig. 2. (a) Close-up photograph of the MLA-mounted MEMS stage. (b) Top view of the MEMS scanner. (c) Scanning electron micrograph of the inner frame and its suspension.

II. Device Design and Fabrication

The device consists of two cascaded frames, each suspended by four flexures. The role of the inner frame is to carry the MLA and serve as mechanical isolation between the MLA and the outer frame, where the actuation occurs [1]. A schematic drawing of the whole device is shown in Fig. 2(b). The dimensions of the outer frame are 4.2 mm $\times$ 2.0 mm, and its four flexures are all parallel, each of which is 800 μm long and 10 μm wide. The outer frame is perforated with holes to decrease the weight and air friction and thus increase the effective quality factor in ambient actuation. The inner frame measures 1.15 mm $\times$ 0.3 mm. The suspension of the inner frame by four flexures, two of which have folded spring geometry, is designed to form stiffness against undesired modes.

The vibration modes of interest for the device are in-plane sliding (translation occurs along the x-axis) and out-of-plane bending (translation occurs along the z-axis) [see Fig. 2(a)]. There are two major goals while engineering the vibration modes: The in-plane sliding mode should be placed as the first mode to enable nonresonant actuation,

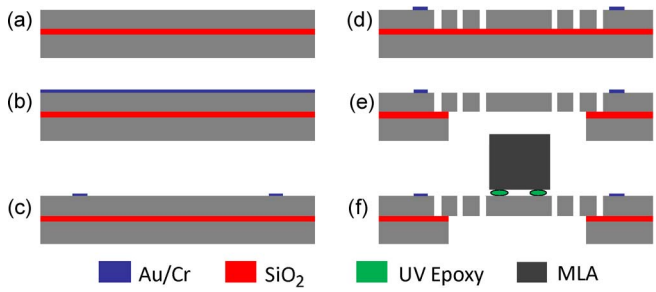

Fig. 3. Three-mask microfabrication process for 2-D MEMS stages.

and the out-of-plane bending mode should be well separated from other vibration modes to avoid unwanted coupling. To achieve this, finite-element method (FEM) software was used to predict the modes of the structure, and in-plane and out-of-plane mode frequencies with the MLA are estimated as 1043 and 3870 Hz, respectively. If the outer frame can be made heavier, one can also achieve a mechanical gain between two frame deflections, which helps avoid comb-capacitance fluctuations due to the large out-of-plane motion of the stage. The mechanical gain in this case was limited to < 2. The simultaneous 2-D actuation of the MLA stage is achieved by superposition of two different drive signals. The low-frequency in-plane motion is actuated out of resonance, while the MLA stage at the same time is vibrating out of plane at the resonance frequency of the out-of-plane bending mode.

The devices were fabricated using a three-mask process for silicon-on-insulator wafers with a 380-μm-thick handle layer, a 2-μm-thick buried oxide (BOX), and a 50-μm device layer. The latter determines the thickness of the entire mechanical structure. The fabrication steps are shown in Fig. 3. At the start of the process, Au/Cr (130/15 nm) is blanket deposited onto the device side of the wafer by sputtering see [Fig. 3(b)]. Mask 1 is used to pattern the metal needed for wire bonding and electrical connections [see Fig. 3(c)]. Mask 2 is used for front-side device definition and Mask 3 for backside windowing [see Fig. 3(d) and (e)]. The silicon etch for the two latter steps is carried out by deep reactive ion etch. They both use the BOX as the etch stop. The final device release is achieved through oxide etch in HF vapor. After dicing, hybrid integration of the MLA on the MEMS stage is performed with manual microstages, using UV epoxy as adhesive [see Fig. 3(f)]. Since the MLA is manually mounted, there will always be some misalignment, which can lead to undesired modes. The 1.1 mm $\times$ 1.1 mm MLAs have 100% fill factor and are fabricated using a glass mold prepared with isotropic etching, from which the pattern is transferred to a layer of UV-curing epoxy.

III. Experimental Result and Discussion

The resonance modes of the devices are located with a laser Doppler vibrometer (Polytec OFV-2500 and OFC-534). There is a generally good agreement between the FEM analysis and the experimentally found modes for devices with or without MLAs. For the mounted devices, there is, however, a large variation from device to device in the location of the modes.

The measurements were carried out on two different mounted devices, A and B. The frequency response for the out-of-plane motion of Device A is shown in Fig. 4. Due to the nonlinear forcing function, the out-of-plane motion behaves as a nonlinear parametric oscillator. It can be actuated at subharmonic frequencies located at $2f_r/n$, where f_r is the mechanical resonance frequency of the system and n is a positive integer [17]. The actual motion of the oscillator will, in all cases, be close to f_r, but the amplitude will increase with decreasing n. The largest deflections are achieved when actuated with a positive square wave at a frequency of $2f_r$. Second, a characteristic hysteretic

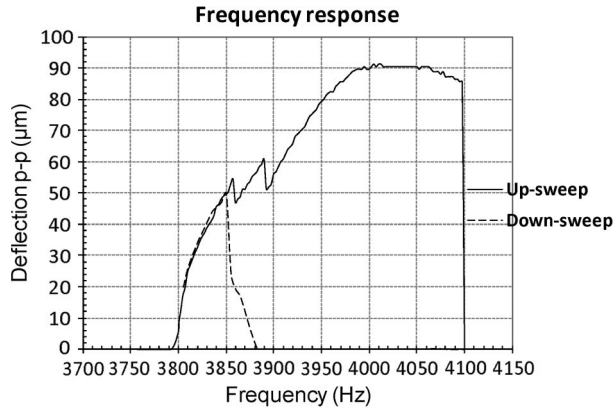

Fig. 4. Vibration frequency response for upsweep and down-sweep for the out-of-plane mode of Device A using a p–p 112-V excitation voltage at twice the vibration frequency. The zigzag pattern below the peak is due to an unexpected resonance mode caused by the manual mounting of the MLA.

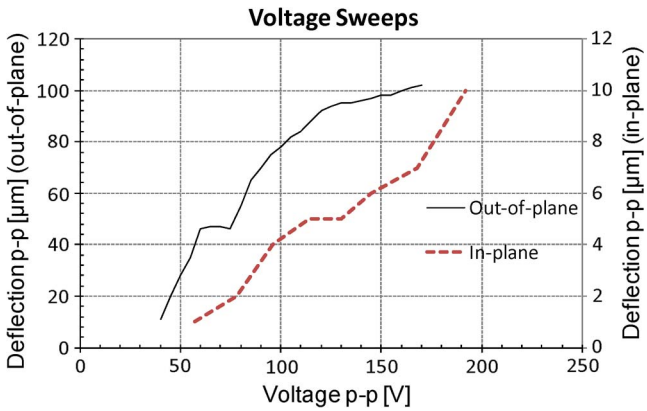

Fig. 5. Voltage response of Device A for (solid curve) in-plane and (dashed curve) out-of-plane actuation. For the in-plane deflection, the frequency is adjusted at each voltage level to achieve the maximum deflection. Out-of-plane deflection is measured at 1 Hz (off resonance).

frequency response is expected for parametric systems, with very different frequency response curves for upsweep and down-sweep. In the figure, there is an unexpected coupling close to the out-of-plane resonance peak. This is attributed to the imperfect mounting of the MLA.

The resonant actuation of Device B at 1927 Hz resulted in a peak-to-peak (p–p) 34-μm deflection for the in-plane resonance mode. For the same device, a 124-μm p–p deflection was measured at the out-of-plane mode, using 100 V at 4193 Hz. For Device A, a p–p 102-μm deflection was achieved at 4606 Hz using 170 V at the out-of-plane mode. The reason for the large discrepancies in the amplitude and the resonance frequency between the two devices can again be attributed to the uncertainties in the manual mounting of the MLA. The voltage responses for the in-plane and out-of-plane deflections of Device A are shown in Fig. 5. For the in-plane actuation at 1 Hz (off resonance), a 10-μm p–p deflection is achieved at 192 V.

An important aspect of this device is that two motions can be actuated simultaneously by superposing two signals applied to the comb drive. This was validated with a device without the MLA, where the resonant frequencies are higher. The device moved simultaneously 45 μm out of plane (at 6 604 Hz) and 13 μm in plane (at 2455 Hz).

To achieve laser beam steering, a stationary MLA is placed two focal lengths away from the MLA mounted onto the stage (see Fig. 1). When the stage is vibrating, a laser beam can be scanned. The resulting scanline can be seen in Fig. 6.

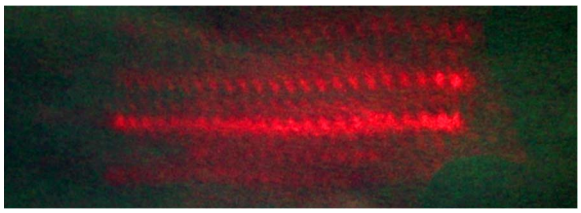

Fig. 6. Scanline achieved by the out-of-plane motion of Device A.

In conclusion, we demonstrated two-axis motion with a MEMS stage using only one uniaxial set of combs. The mechanical design allows for a small device footprint and a large optical clear aperture. The MLA beam steering approach does not suffer from dynamic deformation and can, thus, be implemented with thin substrates. The device can serve as a MOEMS building block in high-resolution beam steering applications. As future work, increasing the mechanical coupling ratio to about ten would significantly reduce the cross coupling between the two axes of motion, rendering simultaneous 2-D motion more efficient. The mounting of the MLA can also be improved to avoid undesired modes.

ACKNOWLEDGMENT

The microfabrication described in this letter was performed in the Center of Micronanotechnology, Ecole Polytechnique Federale de Lausanne, Lausanne, Switzerland. Furthermore, the authors would like to thank C. Ataman for the important prior work and ongoing support, N. Simonian, B. Lunardi, and J.-B. Bureau for the contributions to the process development, and P. Fluckiger and Y. Leblebici for the support and help.

REFERENCES

[1] A. Arslan, W. Davis, D. Brown, S. Holmstrom, S. K. Gokce, and H. Urey, "Comb-actuated resonant torsional microscanner with mechanical amplification," *J. Microelectromech. Syst.*, vol. 19, no. 4, pp. 936–943, Aug. 2010.

[2] S. K. Gokce, S. Holmstrom, C. Hibert, C. Ataman, A. Arslan, H. R. Seren, and H. Urey, "MEMS stage integrated with microlens arrays for high-resolution beam steering," *Proc. Chem.*, vol. 1, no. 1, pp. 1319–1322, Sep. 2009.

[3] A. D. Yalcinkaya, H. Urey, D. Brown, T. Montague, and R. Sprague, "Two-axis electromagnetic microscanner for high resolution displays," *J. Microelectromech. Syst.*, vol. 15, no. 4, pp. 786–794, Aug. 2006.

[4] W. Piyawattanametha, H. Ra, M. J. Mandella, K. Loewke, T. D. Wang, G. S. Kino, O. Solgaard, and C. H. Contag, "3-D near-infrared fluorescence imaging using an MEMS-based miniature dual-axis confocal microscope," *IEEE J. Sel. Topics Quantum Electron.*, vol. 15, no. 5, pp. 1344–1350, Sep./Oct. 2009.

[5] S. Hsu, T. Klose, and Schenk, "Fabrication and characterization of a dynamically flat high resolution micro-scanner," *J. Opt. A, Pure Appl. Opt*, vol. 10, no. 4, p. 044 005, Mar. 2008.

[6] C. Drabe, R. James, H. Schenk, and T. Sandner, "MEMS-devices for laser camera systems for endoscopic applications," *Proc. SPIE*, vol. 7594, p. 759 404, Feb. 2010.

[7] A. Akatay, C. Ataman, and H. Urey, "High-resolution beam steering using microlens arrays," *Opt. Lett.*, vol. 31, no. 19, pp. 2861–2863, Oct. 2006.

[8] J. Duparré, D. Radtke, and P. Dannberg, "Implementation of field lens arrays in beam-deflecting microlens array telescopes," *Appl. Opt.*, vol. 43, no. 25, pp. 4854–4861, Sep. 2004.

[9] H. Miyajima, K. Murakami, and M. Katashiro, "MEMS optical scanners for microscopes," *IEEE J. Sel. Topics Quantum Electron.*, vol. 10, no. 3, pp. 514–27, May/Jun. 2004.

[10] A. Tuantranont, V. M. Bright, J. Zhang, W. Zhang, J. A. Neff, and Y. C. Lee, "Optical beam steering using MEMS-controllable microlens array," *Sens. Actuators A, Phys.*, vol. 91, no. 3, pp. 363–372, Jul. 2001.

[11] S. Kwon, V. Milanovic, and L. P. Lee, "Large-displacement vertical microlens scanner with low driving voltage," *IEEE Photon. Technol. Lett.*, vol. 14, no. 11, pp. 1572–1574, Nov. 2002.

[12] K. Laszczyk, S. Bargiel, J. Krezel, C. Gorecki, and M. Kujawinska, "Silicon comb-drive X-Y microstage with frame-in-the-frame architecture for MOEMS applications," *Proc. SPIE*, vol. 7362, p. 736 210, May 2009.

[13] L. Liu, L. Wu, P. Zory, and H. Xie, "Fiber-optic confocal microscope with an electrothermally-actuated, large-tunable-range microlens scanner for depth scanning," in *Proc. IEEE 23rd Int. Conf. Micro Electro Mech. Syst.*, Hong Kong, 2010, pp. 827–830.

[14] A. Akatay and H. Urey, "Design and optimization of microlens array based high resolution beam steering system," *Opt. Express*, vol. 15, no. 5, pp. 4523–4529, Apr. 2007.

[15] W. C. Tang, M. G. Lim, and R. G. Howe, "Electrostatic comb drive levitation and control method," *J. Microelectromech. Syst.*, vol. 1, no. 4, pp. 170–178, Dec. 1992.

[16] C. Ataman, H. Urey, and A. Wolter, "A Fourier transform spectrometer using resonant vertical comb actuators," *J. Micromech. Microeng.*, vol. 16, no. 12, pp. 2517–2523, Oct. 2006.

[17] K. L. Turner, S. A. Miller, P. G. Hartwell, N. C. MacDonald, S. H. Strogatz, and S. G. Adams, "Five parametric resonances in a microelectromechanical system," *Nature*, vol. 396, no. 6707, pp. 149–152, Nov. 1998.

Annealing Temperature-Dependent Interfacial Behavior of Sequentially Plasma-Activated Silicon Bonded Wafers

Matiar M. R. Howlader, Fangfang Zhang, and Moon J. Kim

***Abstract*—The annealing effects of voids, amorphous layer, and bonding strength in the sequentially plasma-activated silicon/silicon bonded interface were investigated. The interfacial silanol groups and water were condensed and removed, respectively, below and above annealing at 150 °C. About 400 °C, the bonding strength was reduced because of the increased void density associated with the plasma-induced surface defects and the increased thickness of interfacial silicon oxide. The increase of the interfacial thickness layer after annealing was confirmed by high-resolution transmission electron microscope and detected as silicon oxide using the electron energy loss spectroscopy. The surface roughness and contact angle were measured to explain the influence of plasma processing parameters on the interfacial behavior after annealing. While the water contact angle increased with the increase in the O_2 reactive ion etching (RIE) time, the surface roughness was initially decreased and then increased. The surface activation with 400-W O_2 RIE plasma induced defect sites such as nanopores and craters. This study indicates that the O_2 RIE plasma time and power have to be as low as possible to reduce surface roughness and defects but have to be high enough to properly activate the surface with enough surface energy to achieve high quality of Si/Si interface. [2010-0124]**

***Index Terms*—Annealing, electron energy loss spectroscopy (EELS), interfacial amorphous layer, sequentially plasma-activated bonding (SPAB), surface roughness, void density, water contact angle.**

Manuscript received April 30, 2010; revised August 10, 2010; accepted October 13, 2010. Date of publication November 22, 2010; date of current version February 2, 2011. This work was supported in part by the Natural Science and Engineering Research Council of Canada under Discovery Grant 327947 and in part by the Canada Foundation for Innovation under Infrastructure Grant 12128. Subject Editor F. Ayazi.

M. M. R. Howlader and F. Zhang are with the Department of Electrical and Computer Engineering, McMaster University, Hamilton, ON L8S 4K1, Canada (e-mail: mrhowlader@ece.mcmaster.ca).

M. J. Kim is with the Department of Materials Science and Engineering, University of Texas at Dallas, Richardson, TX 75080 USA.

Color versions of one or more of the figures in this paper are available online at http://ieeexplore.ieee.org.

Digital Object Identifier 10.1109/JMEMS.2010.2090502